Journal Name

ARTICLE

Self Limiting Atomic Layer Deposition of Al$_2$O$_3$ on Perovskite surfaces: A Reality?

Devika Choudhury[a], Gopalan Rajaraman[b] and Shaibal K. Sarkar[a*]

The feasibility of self-saturated atomic layer deposition on organo lead halide perovskite (MAPbI$_x$Cl$_{3-x}$) surface through a well known trimethylaluminium (TMA) - water (H$_2$O) chemistry is studied. Though the sequential dosages of reactants form films on the perovskite surfaces but a self saturated growth is never observed. Self-saturation leads to the degradation of the material. Both experimental and density functional theory calculations are carried out for complete understanding of the growth mechanism of self-limiting Al$_2$O$_3$ on the perovskite surface.

Introduction

Hybrid organic-inorganic metal halide perovskite compounds have shown remarkable growth and attracted considerable attention since the pioneering work of Miyasaka et al.[1] in 2009. These compounds have emerged as efficient light harvesters under *p-i-n* configuration and are able to challenge the existing Silicon photovoltaic technologies in terms of high efficiency and cheap cost of production.[2] They exist in both planer[3, 4] and mesoscopic architecture[5, 6] forms where the perovskite absorber is sandwiched between the electron and hole transport layers. Owing to the high carrier lifetime and/or long diffusion length in the perovskite materials, hole transport medium (HTM) free devices have also been developed recently.[7-9] Though HTM free cells are yet to be at par in terms of net conversion efficiency, the simplicity of such device has certainly attracted considerable attention.

Relatively improved device performance of such HTM free cells is observed when atomic layer deposition (ALD) grown Al$_2$O$_3$ is used on perovskite as metal-insulator-semiconductor structure at the back contact.[10] On a similar note, it was demonstrated by Dong et. al that a nanometer thin ALD grown Al$_2$O$_3$ not only helps improve the device efficiency but also subsequently enhances the interface recombination and stability of the device.[11] Thus, through limited resources, it is very much understandable that ALD grown sub-nanometer thickness of the interface layer has a predominant effect on the device performance, especially, of hole-conductor free hybrid perovskite devices.

Self-saturating and surface-limited reaction enables ALD to coat conformally on favoured functionalized surface contour with precise thickness control, ideally atomic.[12] Technically, ALD is a modified chemical vapour deposition (CVD) process where the major characteristic that separates ALD from CVD is the self limiting growth behaviour. Here, the individual chemicals dosed into the reaction chamber sequentially limit the deposition only through surface limited chemical reactions. Thus a complete monolayer formation of the precursor molecule is indeed needed, which is most essential when thinner films (quantum tunnelling regime) are concerned. Unsaturated substrate surface leads to island like growth which certainly compromises on the conformality of the deposited films. Hence any electronic characteristic through a non-conformal discrete film always remains questionable. Therefore, only the sequential dosing of the reactants never actually justifies the process as ALD, rather a combination with the self-limiting surface-limited reaction should be demonstrated to justify the ALD mechanism on any surface.

In this article, we aim to answer whether the scientific philosophy regarding ALD nature of growth of Al$_2$O$_3$ is satisfied on perovskite substrates or not. We relied on the well established TMA-H$_2$O (trimethylaluminum-water) chemistry to deposit Al$_2$O$_3$ by ALD on perovskite. *In-situ* quartz crystal microbalance (QCM), fourier transform infrared (FTIR) spectroscopy and residual gas analyzer (RGA) were used to study the surface limited reaction mechanism during the Al$_2$O$_3$ ALD process. Our experimental findings were supported by density functional theory (DFT) based calculations.

Experimental

Deposition of Perovskite films

Both spin coating method and thermal co-evaporation method were utilised to deposit CH$_3$NH$_3$PbI$_x$Cl$_{3-x}$ on various substrates used for different studies. Spin coating of the PbCl$_2$-

a. Department of Energy Science and Engineering, Indian Institute of Technology Bombay, Mumbai-400076, India
b. Department of Chemistry, Indian Institute of Technology Bombay, Mumbai-400076, India

Methylammonium iodide solution was done on glass substrates having 1μm spin coated porous alumina in a single step at 2000 rpm for 60 seconds. The same solution was used to deposit perovskite films on ALD- Al_2O_3 (30nm) coated KBr pellets used for FTIR studies. In this case, the solution was spin coated in a two step process at 250 rpm and 750 rpm for 5 seconds and 25 seconds respectively on the pellets. All substrates (glass as well as KBr pellets) were heated for 1 hr at 90°C on a hot plate. The entire process of sample preparation was carried out inside a glove box. Furthermore, co-evaporation of CH_3NH_3I and $PbCl_2$ was carried out to deposit $CH_3NH_3PbI_xCl_{3-x}$ on AT-cut 6MHz gold crystal for QCM studies.

Atomic Layer Deposition of Al_2O_3

Al_2O_3 deposition was carried out in a custom built ALD reactor using trimethylaluminum (Sigma Aldrich) and water (HPLC grade, Merck) as precursors. Both precursors were used as received and maintained at room temperature. The differential pressures of the precursor doses were measured with a capacitance manometer, Baratron (MKS instruments). All depositions were carried out at 75°C under constant N_2 flow of 0.9Torr. Precursor exposures were controlled using computer controlled pneumatic valves.

Growth study was done with *in situ* QCM setup. A 6 MHz AT-cut gold coated crystal was inserted into a crystal and drawer assembly (from Inficon) and sealed with non-conducting silver paste. $CH_3NH_3PbI_xCl_{3-x}$ perovskite was deposited on the crystal by co-evaporation of CH_3NH_3I and $PbCl_2$. Once deposited, the whole assembly was inserted into the viscous flow type ALD reactor maintained at 75°C. A pressure of 0.9Torr was maintained inside the reactor with continuous N_2 flow. An additional positive pressure of 0.1Torr was also maintained to prevent any deposition on the reverse side of the crystal. An Inficon SQM160 monitor detects the frequency change of the crystal which is then converted to mass change using the Sauerbrey Equation. A positive increase in mass depicts a mass gain on the crystal while a negative increase in mass depicts a mass loss from the crystal.

Characterisations

In-situ FTIR was utilized to study the surface chemistry during the exposures of TMA, H_2O and deposition of Al_2O_3 on the perovskite films. All depositions were carried out in a different ALD reactor similar to the previously described one but additionally equipped with ZnSe windows. IR beam is passed through the windows and detected with liquid nitrogen cooled cadmium telluride detector. Vertex 70 FTIR instrument from Bruker was used to perform the *in-situ* FTIR measurements. Spectrums were acquired over an average of 100 scans with a resolution of 4cm^{-1}. XRD patterns were acquired using a Rigaku Smartlab X-Ray diffractometer equipped with a Cu-Kα source (1.54Å). Residual gas analysis of the byproducts was done with the help of Transpector compact process monitor from Inficon having 70eV of ionisation energy.

Computational details

All DFT calculations were done using Gaussian 09[13] suit of programs. Since the interaction involved between the fragments are weak intermolecular interaction, here M06[14] suite of functional was employed along with LANL2DZ[15] basis set to describe the heavier Pb and I atoms, whereas 6-311G++(d,p) basis set was used to describe all the other atoms. All the reported energies are the optimized zero point energy corrections obtained from calculations.

Results and Discussions

Atomic Layer deposition of Al_2O_3 was carried out following the well established ALD chemistry of two half surface reactions: [16-18]

(A) $Al-OH* + Al(CH_3)_3* \rightarrow Al-O-Al(CH_3)_2* + CH_4$
(B) $Al-CH_3* + H_2O \rightarrow Al-OH* + CH_4$
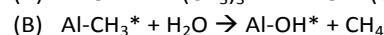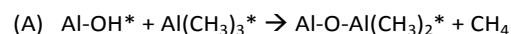
Here, all the deposition was done between 75°C to 80°C due to the thermal instability of perovskite at higher temperatures. Alternate dose of TMA and H_2O were introduced into the reactor in the sequence 1s-30s-1s-30s. Here 1s is the dose time in seconds for alternate TMA and H_2O doses while 30s is the purge time between each successive precursor exposures. The $CH_3NH_3PbI_xCl_{3-x}$ (MAPbICl) film was deposited either by co-evaporation or spin coating methods as described earlier.
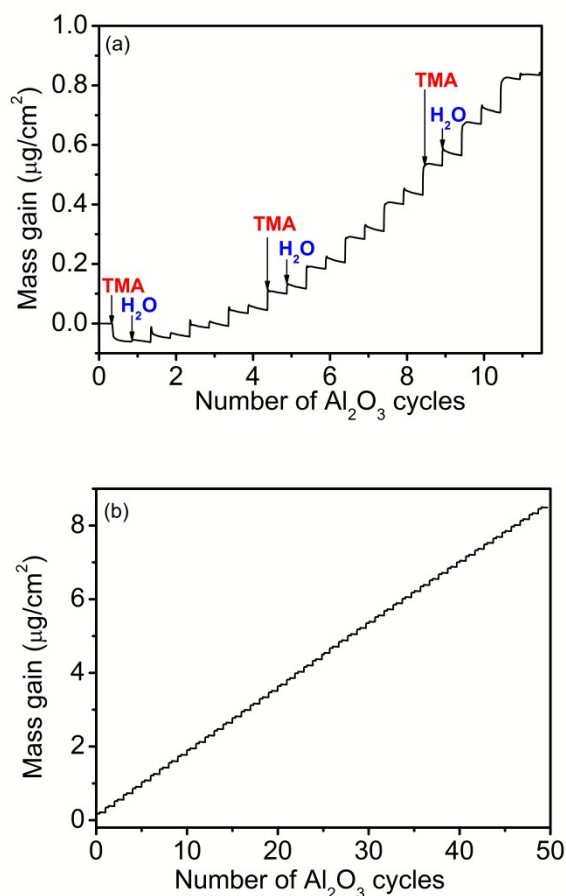
Fig. 1 Nucleation and growth of Al_2O_3 grown on perovskite surface at 75°C studied by *in-situ* QCM, (a) Initial 10 cycles, (b) successive 50 cycles of ALD-Al_2O_3 on perovskite.

Fig. 1a and Fig. 1b show the mass change as measured during the first 10 cycles and successive 50 cycles respectively of Al_2O_3 deposition, using QCM during the growth of Al_2O_3 on perovskite coated qcm surface. Fig. 1a shows an initial non-linear growth regime of Al_2O_3 growth on perovskite surface while a linear growth is observed subsequently as shown in fig. 1b. The continuous linear mass change as a function of the deposition cycle time (as seen from fig. 1b) is as typical to any thin film growth in ALD. The average mass change of Al_2O_3 per cycle here is found to be approx. 170 ng per ALD cycle which is much higher than that reported in literature.[18] The higher mass gain per cycle can be attributed to the roughness that effectively increases the net geometric area of the $MAPbI_xCl_{3-x}$ films deposited by thermal co-evaporation on the crystal surface.

On a further closer look, at the initial few cycles of the Al_2O_3 growth, as shown in fig. 1a, two interesting phenomenon are noticed,

(a) The non-linear mass change per ALD cycle that can be well attributed to the nucleation regime of the growth process, as mentioned earlier, and
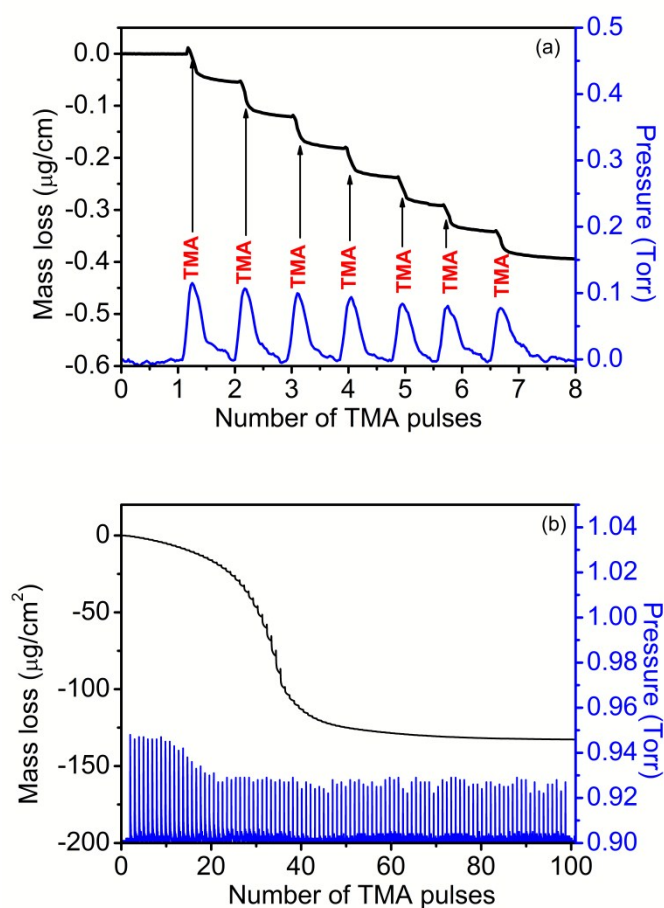
(b) Mass decrease upon first dose of the TMA.

Fig. 2 (a) Initial mass change and (b) complete mass change characteristic due to successive TMA exposure on perovskite surface as measured by QCM.

A trivial nucleation regime of a few ALD cycles is observed due to the non-hydroxilated surface of the perovskite. However, an important fact that needs to be elucidated here is the mass decrease during the first TMA dose, which is never expected even on a non-hydroxilated surface like as this. Such decrease in mass indicates etching out of the surface species. Furthermore, when a train of TMA consecutive pulses are dosed, a subsequent mass loss on every cycle is noticed, as shown in the fig. 2a. This mass decrease per dose of TMA is also found to be limited by the available surface sites as noticeable from fig. 2b. Upon continuous TMA exposure etching rate increases due to the continuous evolution of reactive surface sites resulting in an enhanced rate of mass loss. This is observed beyond 20-25 cycles of TMA exposures. Furthermore beyond ca. 35 dosages of TMA a decrease in the rate of "etching" is observed again which is probably due to the limited availability of the surface sites then. This certainly proves the fact that no surface saturation of the TMA can ever be obtained on the perovskite surface.

These "yellow" films as compared to the original blackish brown colour obtained upon continuous exposure of TMA dosages on $MAPBI_{3-x}Cl_x$ films were further investigated with X-ray diffraction (XRD) measurements and compared with the original perovskite structure. Fig. 3a shows the XRD of only perovskite film spin coated on KBr pellet. The diffraction pattern of the initial perovskite film corresponding to $CH_3NH_3PbI_2Cl$ is similar to the available literature.[19] Peaks at 14.1°, 28.4° and 43.2° correspond to the (110), (220) and (330) planes respectively of a tetragonal perovskite structure. The additional peaks at 23.3°, 27.0°, 38.5°, 45.6°, 47.6° and 55.6° all correspond to the KBr substrate. Fig. 3b on the other hand shows the XRD pattern of the same film after continuous TMA exposure.
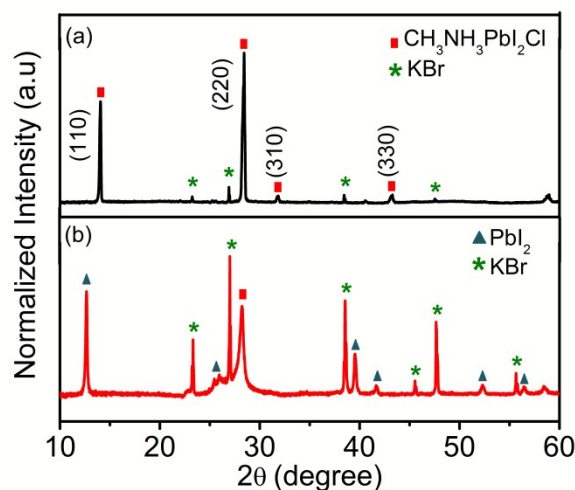

Fig. 3 X-ray diffraction (XRD) pattern of (a) as-deposited $CH_3NH_3PbI_xCl_{3-x}$ film, (b) $CH_3NH_3PbI_xCl_{3-x}$ film after continuous TMA exposure, both on KBr pellet.

As observed from fig. 3b, majority of the characteristic peaks of $MAPbI_{3-x}Cl_x$ become non-existent in the TMA exposed perovskite film. The XRD spectrum of the exposed film is found to match with PbI_2 (JCPDS File No.-01-073-1750). The peak positions at 12.6°, 25.9°, 39.4°, 41.6°, 52.3° and 56.5° correspond to the (001), (011), (110), (111), (004) and (113)

planes of PbI$_2$ respectively. This is also in complete resemblance to the yellow colouration of PbI$_2$ material.

To further understand the chemical nature of the degradation of MAPbI$_{3-x}$Cl$_x$, in-situ FTIR spectroscopy studies were performed. Fig. 4a shows the FTIR spectra of MAPbI$_{3-x}$Cl$_x$, deposited on KBr pellet, during exposure to consecutive doses

Wavenumber (cm^{-1})		Assigned Vibration mode
Experimentally obtained	Theoretically obtained	
3166	3159	N-H stretch
3130	3140	N-H stretch
2958	3055	C-H stretch
1584	1593	N-H bend
1469	1468	C-H bend
1248	1259	C-N stretch
917	935	C-N stretch

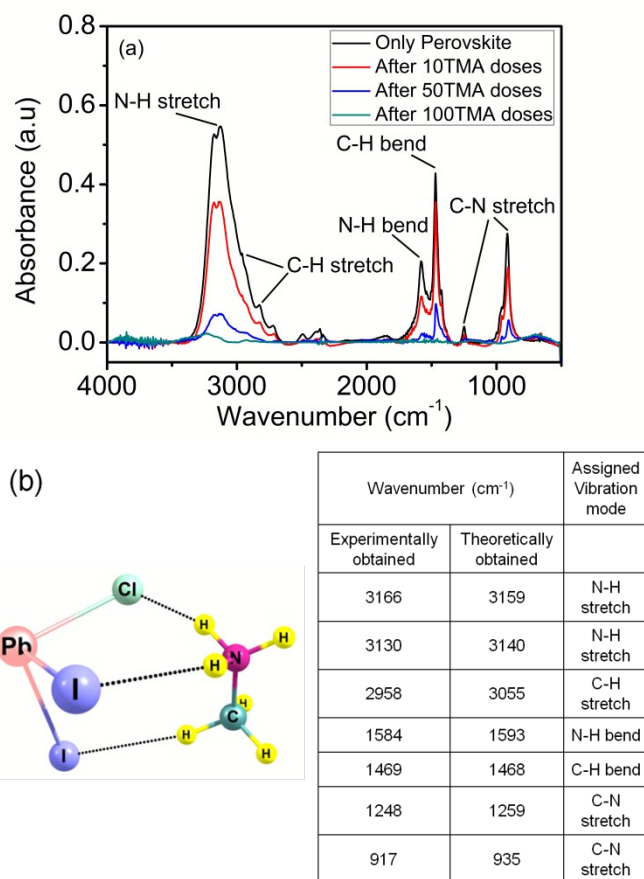**Fig. 4** (a) FTIR spectra of perovskite and the change observed upon continuous exposure to TMA, (b) Optimized structure of MAPbI$_{3-x}$Cl$_x$ obtained from DFT calculation.

of TMA under vacuum. The vibrational modes of only perovkite film thus obtained are closely similar to earlier reports.[20] The N-H stretch lies within the range 3,100-3,450 cm^{-1} while the C-H stretches exists within 2,800-2,950 cm^{-1}. Furthermore, N-H and C-H bend are found within the range 1,300-1600 cm^{-1} while the C-N stretch is found to be at approximately 900-1000cm^{-1} as seen from the calculated FTIR spectrum. Experimentally determined peaks reasonably matches well to the one obtained from DFT calculation as depicted in the fig. 4b. As seen in fig. 4a, with increase in TMA exposure, the net absorbance of various vibrational modes gradually reduces and beyond 100 TMA doses, no signature peaks of MAPbI$_{3-x}$Cl$_x$ are found. Again appearance of any new peaks is also not observed. Interestingly, similar observation is found when only MAI is exposed to consecutive dosages of TMA while for PbI$_2$ no considerable change in the spectrum is noticed (shown in fig. S1 in SI).

It is mentionworthy at this point that knowing its instability under humid ambience, similar degradation is expected upon exposing the perovskite to H$_2$O dosages. However, consecutive H$_2$O exposures of 5x10^{6}L, typically used for ALD growth of Al$_2$O$_3$, though results in some observable reduction in IR absorption peak intensities (shown in fig. S2a in SI) during the course of the experimental time frame but is surprisingly significantly lower in comparison to that resulted from the TMA doses. Similarly, sequential doses of TMA and H$_2$O, which result in the growth of Al$_2$O$_3$, also show no observable degradation under FTIR (Fig. S2b in SI), only an increase in the Al-O stretch is observed.

Analysis of the byproducts obtained during the reaction of TMA on perovskite was performed with RGA. The aim was to qualify the volatile products during the reaction that certainly helped to understand the detailed reaction mechanism between TMA and MAPbI$_x$Cl$_{3-x}$. RGA spectrum analysis reveals the elimination of CH$_4$ and CH$_3$NH$_2$ from the perovskite surface (shown in fig. S3 in SI and explained). This probabilistically satisfy the findings from XRD and FTIR analysis where decrease in the organic moeity from the perovskite material results in the nonvolatile residual PbI$_2$.

The RGA analysis thus helps to hypothesize the mechanistic pathway between TMA and CH$_3$NH$_3$PbI$_x$Cl$_{3-x}$. To confirm the probable reaction mechanism, density functional theory analysis was carried out. It is to be mentioned here that following two approximations were considered for all calculations:

(a) CH$_3$NH$_3$PbI$_x$Cl$_{3-x}$ perovskite is nothing but CH$_3$NH$_3$PbI$_3$ with the presence of Cl as a dopant.[21] Thus to simplify the DFT calculations and to probe the probable mechanism in detail, the perovskite structure henceforth is considered as simple CH$_3$NH$_3$PbI$_3$.

(b) Earlier reports mention that TMA exists in an equilibrium of monomer and dimer in the gaseous state, with the probability of the presence of dimer being higher at lower temperatures (approx. 70C),[22,23]. As all the experiments were carried out in the similar temperature range, calculations between perovskite and TMA were done using both TMA monomer and TMA dimer.

Similar to the earlier reports, our DFT calculations also reveal strong intermolecular interaction between PbI$_3^-$ anion and the CH$_3$NH$_3^+$ cation in the perovskite structure.[11] When TMA (both dimer and monomer) reacts with the perovskite structure, CH$_4$ and CH$_3$NH$_2$ are eliminated as byproducts as obtained from the RGA analysis. It must be mentioned that three different mechanistic scenarios are tested here,

(a) bridging –CH$_3$ group of TMA dimer reacts with the –NH group of perovskite leading to the products mentioned above,

(b) terminal –CH$_3$ group of TMA dimer reacts with the –NH group of perovskite leading to the products mentioned above,

(c) one of the –CH$_3$ group of TMA monomer reacts with the –NH group of perovskite leading to the products mentioned above.

Journal Name

ARTICLE
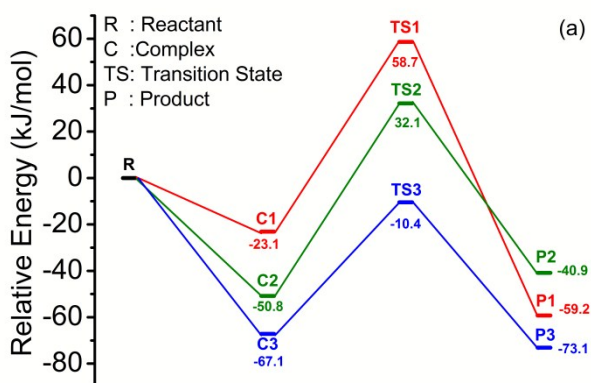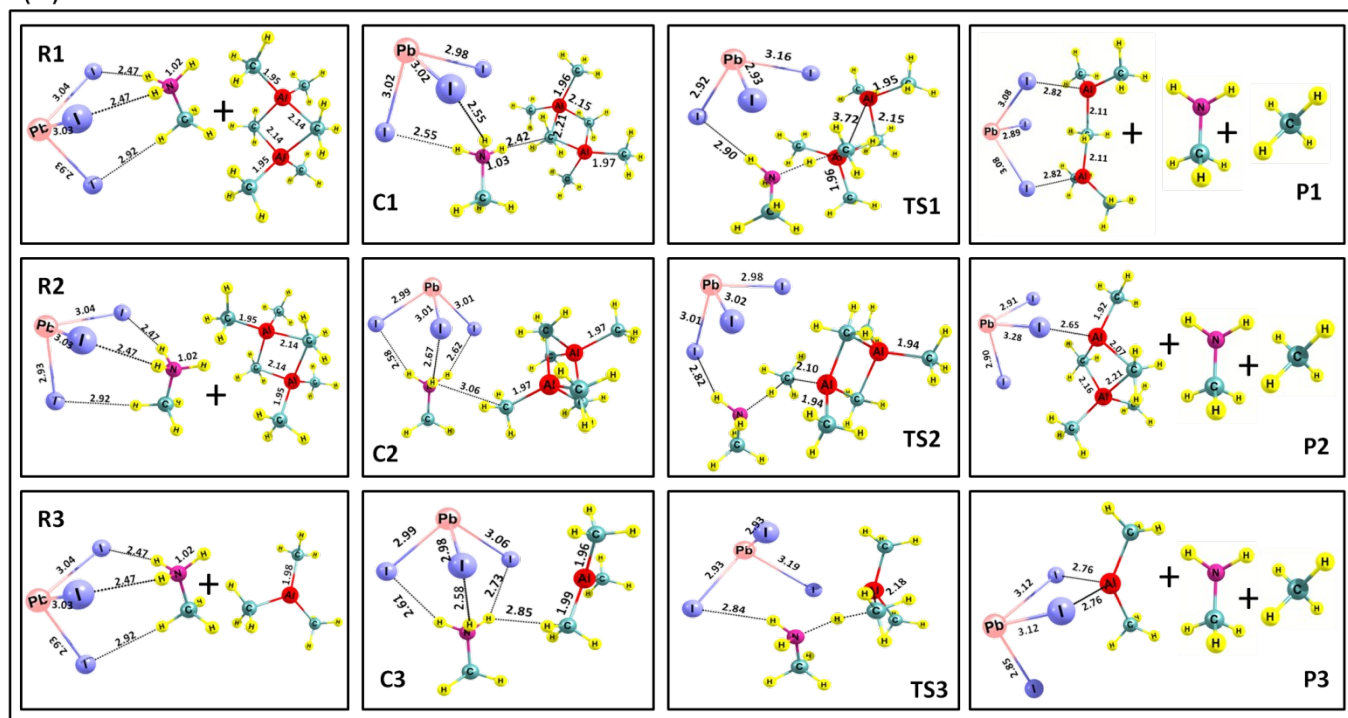
Fig. 5 (a) Reaction pathways and calculated energies for reactions between CH$_3$NH$_3$PbI$_3$ and (1), (2) TMA dimer, and (3) TMA monomer, (b) obtained optimized structures for each step of the reaction pathways with bond lengths in Angstorm.

Fig. 5 shows the various optimization structures for the reaction between perovskite and TMA for (a), (b) and (c) approaches.

For all the pathways, the TMA (monomer/dimers) are expected to interact with the CH$_3$NH$_3$PbI$_3$ unit leading to the formation of a weak complex (C1-C3). As pathway a-c assumes

formation of CH$_4$ from different methyl groups, the orientation of TMA (monomer/dimer) with the CH$_3$NH$_3$PbI$_3$ differs (shown in Fig. 5b). In the next step the H-atom abstraction from the CH$_3$NH$_3$$^+$ cation is assumed to take place leading to the formation of CH$_4$ and CH$_3$NH$_2$ byproducts (P1-P3).

The potential energy surfaces (PES) of fig. 5a shows that the bridging CH_3 group of TMA dimer reacts with perovskite thus forming a product of PbI_3-$Al(CH_3)_5$ with the simultaneous release of CH_4 along with CH_3NH_2 resulting in the release of 59.2 kJ/mol of energy (along the R-C1-TS1-P1 path).

Similarly, the –CH_3 group of TMA monomer also reacts with the formation of PbI_3-$Al(CH_3)_2$ and release of the same byproducts with an energy of 73.1 kJ/mol (pathway 'c', R-C3-TS3-P3). Pathway 'b' (R-C2-TS2-P2) however resulted in overall exothermicity much lower than the others (-40.9 kJ/mol). A similar trend was observed also with UB3LYP functional (as shown in fig. S4 in SI) reflecting a fact that the results are not strongly dependent on the nature of the exchange correlation functional. The calculations thus reveal that TMA (either existing as dimer or monomer) reacts with perovskite causing breakdown of the perovskite structure. Transition states of the different pathways show that pathway 'c' is a barrier less path from the reactant while pathways 'a' and 'b' have barriers of 58.7kJ/mol and 38.2kJ/mol respectively. This shows that the pathway involving the removal of the terminal –CH_3 molecule of the TMA dimer is more kinetically favoured than removal of the bridging –CH_3 moiety, while the pathway 'c' is the most favourable.

Closer analysis of the optimized structures of reactants (R), complexes (C), transition states (TS) and products (P) (as shown in fig. 5b) gives a better understanding of the formation of adducts with the simultaneous release of CH_3NH_2 and CH_4 as byproducts. Each of the complexes C1, C2 and C3 reveal an increase in the length of the already weak interactions between I and H atoms which forms the perovskite in the first place. This causes further weakening of the interaction betweem PbI_3^- anion and the $CH_3NH_3^+$ cation causing the CH_3NH_2 moiety to break off from the perovskite molecule altogether. Also, one of the H atoms of the $CH_3NH_3^+$ cation experiences a close interaction with the C atom of the –CH_3 group of the TMA dimer/monomer, the distances varying from 2.3 to 3Å. Thus the exclusion of CH_4 clearly shows that the bonding between the PbI_3^- anion and $CH_3NH_3^+$ cation breaks with the release of CH_3NH_2. On continuous dosing of TMA, it can be anticipated that all the perovskite molecules dissociates thus dissolving the total perovskite structure with release of CH_3NH_2 leaving behind PbI_2-adduct with $Al_2(CH_3)_5$ as per calculations. Other pathways were also considered which gave similar or higher optimized energies but similar trends as shown in S5 in SI.

Furthermore, as opposed to the mass loss during the TMA exposure, we find that H_2O exposure resulted in a mass gain, observed by *in-situ* QCM measurements (shown in fig. S7a, SI). Such mass gain during the H_2O exposure is perfectly explained through DFT calculations as well. Our calculations and as well as an earlier report confirm that H_2O molecules form a strong interaction with the $(CH_3NH_3)^+$ cation thus weakening the PbI_3-CH_3NH_3 interaction.[11] However a single H_2O molecule is not sufficient for the breakdown of the perovskite structure. It rather forms a $CH_3NH_3PbI_3.H_2O$ system giving rise to an addition of OH surface sites (shown in fig. S6a). This explains the mass gain after H_2O exposure as

observed in fig. S7a. The –OH surface site thus seeds the possibility of sequential growth of Al_2O_3 on the perovskite surface. Hence, subsequent doses of TMA shows a mass gain instead of the mass loss seen earlier (Fig. S7b in SI). Thus all the subsequent TMA and water doses follow the linear growth behaviour typical for ALD Al_2O_3. However, excess of water dosages results in the deformation of the perovskite molecule as evident from the FTIR spectroscopy. It is found that every perovskite molecule needs two water molecules to break the interactive bonds between the perovskite anion and cation (also shown in fig. S6b in SI).[11] The slow decrease in the FTIR spectra during H_2O exposures can be thus attributed to the slow degradation of the perovskite structure on slower encounter with H_2O molecules in the ALD reactor. The possibility of one or two H_2O molecules reacting with the perovskite surface also explains the nucleation regime observed during the sequential growth of TMA-H_2O as seen earlier in fig. 1a.

All DFT calculations were done undertaking single $CH_3NH_3PbI_3$ molecules due to limited computational resources. Although these molecules do not specifically represent the entire surface of the perovskite films, it is believed that this does not affect the hypothesized reaction mechanism of TMA with $CH_3NH_3PbI_3$. Earlier reports show that ALD reactions mechanisms are fairly insensitive to the cluster sizes used[24-28]. Hence smaller models sufficiently mimic the reaction pathway correctly. An earlier report by one of the authors on interaction of thiols on Au layers also show that number of layers does not play a significant role in the kinetics of the reaction[29]. This provides confidence on our computed energetic using single molecules. However it is highly recommended to perform calculations on surfaces using periodic DFT to gain detailed insight into the role of cooperativity and intermolecular interactions on the kinetics of the reaction.

Conclusion

Our experimental finding hence equivocally suggests that the sequential exposure of TMA and H_2O surely give rise to Al_2O_3 deposition but certainly the reaction chemistry never follows the self saturation criterion of ALD on the perovskite surface. Both the reactants react with the substrate but are kinetically different. Trimethylaluminum reacts with the perovskite surface causing weakening of the intermolecular attraction between the PbI_3^- and $CH_3NH_3^+$ counterparts of the perovskite molecule, thus causing breakdown of the structure. This results in etching of the perovskite surface, never allowing the self-limited monolayer formation after the TMA precursor dose. On the other hand H_2O reacts in either of two ways, (a) either a single H_2O molecule reacts with perovskite that gives rise to few –OH surface sites, or (b) two H_2O molecules react with the perovskite structure resulting in the anticipated dissociation of the perovskite molecule. Again the –OH surface site obtained via "a" can seed the growth of Al_2O_3 on the perovskite surface however whether "a" or "b" pathway will occur is beyond selective control. Hence, though Al_2O_3 film

ARTICLE

deposition is definitely possible on the perovskite surface, the possibility of a conformal, self-saturated ALD growth by TMA-H_2O reaction is not anticipated.

Acknowledgements

References

1   A. Kojima, K. Teshima, Y. Shirai and T. Miyasaka, *J. Am. Chem. Soc*, 2009, **131**, 6050-6051.
2   M. A. Green, A. Ho-Baillie and H. J. Snaith, *Nat Photon*, 2014, **8**, 506-514.
3   J. M. Ball, M. M. Lee, A. Hey and H. J. Snaith, *Energy Environ. Sci*, 2013, **6**, 1739-1743.
4   D. Liu and T. L. Kelly, *Nat Photon*, 2014, **8**, 133-138.
5   J. Burschka, N. Pellet, S.-J. Moon, R. Humphry-Baker, P. Gao, M. K. Nazeeruddin and M. Gratzel, *Nature*, 2013, **499**, 316-319.
6   K. Wojciechowski, M. Saliba, T. Leijtens, A. Abate and H. J. Snaith, *Energy Environ. Sci*, 2014, **7**, 1142-1147.
7   L. Etgar, P. Gao, Z. Xue, Q. Peng, A. K. Chandiran, B. Liu, M. K. Nazeeruddin and M. Grätzel, *J. Am. Chem. Soc*, 2012, **134**, 17396-17399.
8   J. Shi, J. Dong, S. Lv, Y. Xu, L. Zhu, J. Xiao, X. Xu, H. Wu, D. Li, Y. Luo and Q. Meng, *Appl. Phys. Lett*, 2014, **104**, 063901.
9   S. Aharon, S. Gamliel, B. E. Cohen and L. Etgar, *Phys. Chem. Chem. Phys*, 2014, **16**, 10512-10518.
10   H. Wei, J. Shi, X. Xu, J. Xiao, J. Luo, J. Dong, S. Lv, L. Zhu, H. Wu, D. Li, Y. Luo, Q. Meng and Q. Chen, *Phys. Chem. Chem. Phys*, 2015, **17**, 4937-4944.
11   X. Dong, X. Fang, M. Lv, B. Lin, S. Zhang, J. Ding and N. Yuan, *J. Mater. Chem. A*, 2015, **3**, 5360-5367.
12   S. M. George, *Chem. Rev*, 2009, **110**, 111-131.
13   G. W. T. M. J. Frisch, H. B. Schlegel, G. E. Scuseria, M. A. Robb, J. R. Cheeseman, G. Scalmani, V. Barone, B. Mennucci, G. A. Petersson, H. Nakatsuji, M. Caricato, X. Li, H. P. Hratchian, A. F. Izmaylov, J. Bloino, G. Zheng, J. L. Sonnenberg, M. Hada, M. Ehara, K. Toyota, R. Fukuda, J. Hasegawa, M. Ishida, T. Nakajima, Y. Honda, O. Kitao, H. Nakai, T. Vreven, J. A. Montgomery, Jr., J. E. Peralta, F. Ogliaro, M. Bearpark, J. J. Heyd, E. Brothers, K. N. Kudin, V. N. Staroverov, R. Kobayashi, J. Normand, K. Raghavachari, A. Rendell, J. C. Burant, S. S. Iyengar, J. Tomasi, M. Cossi, N. Rega, J. M. Millam, M. Klene, J. E. Knox, J. B. Cross, V. Bakken, C. Adamo, J. Jaramillo, R. Gomperts, R. E. Stratmann, O. Yazyev, A. J. Austin, R. Cammi, C. Pomelli, J. W. Ochterski, R. L. Martin, K. Morokuma, V. G. Zakrzewski, G. A. Voth, P. Salvador, J. J. Dannenberg, S. Dapprich, A. D. Daniels, Ö. Farkas, J. B. Foresman, J. V. Ortiz, J. Cioslowski, and D. J. Fox,, *Gaussian 09, Revision D.01,* , Gaussian, Inc.,, Wallingford CT, , 2009.
14   Y. Zhao and D. Truhlar, *Theor Chem Account*, 2008, **120**, 215-241.
15   A. D. Becke, *J. Chem. Phys*, 1993, **98**, 5648-5652.
16   A. C. Dillon, A. W. Ott, J. D. Way and S. M. George, *Surf. Sci*, 1995, **322**, 230-242.
17   A. W. Ott, J. W. Klaus, J. M. Johnson and S. M. George, *Thin Solid Films*, 1997, **292**, 135-144.
18   M. D. Groner, F. H. Fabreguette, J. W. Elam and S. M. George, *Chem. Mater*, 2004, **16**, 639-645.
19   M. M. Lee, J. Teuscher, T. Miyasaka, T. N. Murakami and H. J. Snaith, *Science*, 2012, **338**, 643-647.
20   N. J. Jeon, J. H. Noh, Y. C. Kim, W. S. Yang, S. Ryu and S. I. Seok, *Nat Mater*, 2014, **13**, 897-903.
21   S. Colella, E. Mosconi, P. Fedeli, A. Listorti, F. Gazza, F. Orlandi, P. Ferro, T. Besagni, A. Rizzo, G. Calestani, G. Gigli, F. De Angelis and R. Mosca, *Chem. Mater*, 2013, **25**, 4613-4618.
22   J. Tanaka and S. R. Smith, *Inorg. Chem*, 1969, **8**, 265-270.
23   D. Berthomieu, Y. Bacquet, L. Pedocchi and A. Goursot, *J. Phys. Chem. A*, 1998, **102**, 7821-7827.
24. Y. Xu and C. B. Musgrave, *Chem. Mater*, 2004, **16**, 646-653.
25. A. Afshar and K. C. Cadien, *Appl. Phys. Lett*, 2013, **103**, 251906(1)-251906(5).
26. Y. Xu and C. B. Musgrave, *Surf. Sci*, 2005, **591**, L280-L285.
27. Y. Widjaja and C. B. Musgrave, *Appl. Phys. Lett*, 2002, **81**, 304-306.
28. C. Mui, Y. Widjaja, J. K. Kang, C. B. Musgrave, *Surf. Sci*, 2004, **557**, 159-170.
29. M. Jaccob, G. Rajaraman and F. Totti, *Theor. Chem. Acc*, 2012, **131**, 1150(1)-1150(11).

Nanoscale Accepted Manuscript